

A constitutive law for rate of earthquake production and its application to earthquake clustering

James Dieterich

U.S. Geological Survey, Menlo Park, California

Abstract. Seismicity is modeled as a sequence of earthquake nucleation events in which the distribution of initial conditions over the population of nucleation sources and stressing history control the timing of earthquakes. The model is implemented using solutions for nucleation of unstable fault slip on faults with experimentally derived rate- and state-dependent fault properties. This yields a general state-variable constitutive formulation for rate of earthquake production resulting from an applied stressing history. To illustrate and test the model some characteristics of seismicity following a stress step have been explored. It is proposed that various features of earthquake clustering arise from sensitivity of nucleation times to the stress changes induced by prior earthquakes. The model gives the characteristic Omori aftershock decay law and interprets aftershock parameters in terms of stress change and stressing rate. Earthquake data appear to support a model prediction that aftershock duration, defined as the time for rates to return to the background seismicity rate, is proportional to mainshock recurrence time. Observed spatial and temporal clustering of earthquake pairs arises as a consequence of the spatial dependence of stress changes of the first event of the pair and stress-sensitive time-dependent nucleation. Applications of the constitutive formulation are not restricted to the simple stress step models investigated here. It may be applied to stressing histories of arbitrary complexity. The apparent success at modeling clustering phenomena suggests the possibility of using the formulation to estimate short- to intermediate-term earthquake probabilities following occurrence of other earthquakes and for inversion of temporal variations of earthquake rates for changes in driving stress.

Introduction

Change of the rate of production of earthquakes is a readily observed and characteristic feature of earthquake occurrence. Physical causes of temporal variations of seismic activity remain poorly understood. However, various attributes of earthquake activity indicate a connection between alteration of stress and earthquake rates. Significant geologic events which modify stress state are often associated with pronounced changes of the rate of production of earthquakes. Examples include aftershocks following large earthquakes, earthquake swarms associated with magma intrusion processes, and systematic variation of background seismicity through the stressing cycle of great earthquakes [e.g., *Ellsworth et al.*, 1981]. Also, changes of effective stress related to impoundment of reservoirs and fluid injection into deep wells are well known to alter seismicity. Finally, at distances generally not associated with aftershocks, *Reasenberg and Simpson* [1992] have reported correlations between small stress changes calculated for the 1989 Loma Prieta, California, earthquake and small changes in the rates of production of background seismicity.

This paper presents a general approach for obtaining rate of earthquake activity resulting from some stressing history. The concept is implemented for faults with rate- and state-dependent constitutive properties which are derived from

laboratory fault slip experiments. Previously, some effects of stress perturbations on rate of earthquake occurrence and earthquake probability have been simulated for faults with these properties [Dieterich, 1986, 1987, 1988b]. Those previous applications employed numerical simulations or limited closed-form solutions. The following presents a general constitutive formulation for rate of earthquake production on faults with rate- and state-dependent friction. The formulation is amenable to exact solution for simple stressing perturbations, and by straightforward numerical implementation it may be applied to stressing histories of arbitrary complexity. To illustrate and test the model some applications to earthquake aftershocks and earthquake clustering are presented. Table 1 lists symbols used in this study and equation numbers where the symbols first appear.

Model

General formulation. In the following discussion the term "earthquake nucleation" is used to describe the processes and interactions that lead to the initiation of an earthquake instability at some specific place and time. Nucleation is assumed to occur over a restricted region which is referred to as a nucleation source. The essential concept of the analysis is the treatment of a seismically active volume of the Earth as having a population of sources that nucleate successive earthquakes to produce observed seismicity. The objective is to find the time at which each source in the population initiates an earthquake by following the evolution of conditions on the sources when subjected to some stressing history.

This paper is not subject to U.S. copyright. Published in 1994 by the American Geophysical Union.

Paper number 93JB02581.

To implement this proposition requires a specific model of the earthquake nucleation process. The general formulation scheme developed in equations (1) through (4) can be employed for various models of the earthquake nucleation process. Constitutive properties and system interactions that provide a mechanism for the onset of unstable fault slip must be specified, giving the time t at which a particular source nucleates an earthquake from initial conditions and stressing history:

$$t = F[C, \tau(t)] , \quad (1)$$

where C represents initial conditions and $\tau(t)$ is some general stressing history. For example, in a model with instantaneous nucleation at a stress threshold, C might be expressed as the initial stress relative to the stress threshold. In this work, which is implemented for a model of time-dependent nucleation by accelerating slip, C is the initial slip speed on the nucleation source.

Changes of stress state within the volume containing the population of nucleation sources may arise from external processes and possibly from earthquakes occurring within the volume. As used here, stressing history may also include changes of effective normal stress brought about by pore pressure changes. The volume is assumed to be sufficiently small that all sources experience the same changes of stress, although conditions, which include initial stress state, will vary over the population of sources.

This work employs the convention of redefining C at the start of every time step in situations where time stepping is employed to follow the evolution of conditions. In general, the distribution of initial conditions at the start of a time increment will be determined by the prior stressing history and the prior distribution. Consequently, a distribution of initial conditions under some reference stressing history is first constructed. In setting up the reference distribution it is assumed that a constant steady state seismicity rate r develops under a condition of constant reference stressing rate $\dot{\tau}_r$. Hence

$$t = n/r \quad (2)$$

where n is the sequence number of the earthquake source and indicates the n th source in the distribution. Although strictly regular seismicity is assumed for construction of the reference distribution, the constant rate r may be interpreted as a statistical measure of expected rate of earthquake production for some magnitude interval (i.e., Poisson model of occurrence). This appears to be the simplest assumption to make for defining the distribution and is supported by some observations [e.g., Wyss and Haberman, 1988]. Alternate assumptions to (2) might be to specify a nonsteady distribution of earthquakes over time, based for example, on models of stress heterogeneity or variation of seismic potential through the cycle of great earthquakes. For the specific implementation developed below, use of steady state rate appears to be adequate, at least over time intervals that are small compared to the mean recurrence time of major crustal earthquakes.

Equating (2) with the specific solution of (1) for the constant stressing rate $\dot{\tau}_r$ gives the distribution of initial conditions that yields the constant reference seismicity rate

$$C = C(n, r, \dot{\tau}_r) . \quad (3)$$

Substituting the distribution of initial conditions into the general solution of (1) gives the distribution of earthquake times for the general stressing history

$$t = F[C(n, r, \dot{\tau}_r), \tau(t)] . \quad (4)$$

Because stressing histories may be rather complicated, involving stress jumps and irregular fluctuations, practical

Table 1. Mathematical Symbols

Symbol	Equation First Used	Description
a, b	(15)	Omori aftershock decay parameters
A, B	(5)	fault constitutive parameters
c	(20)	radius of shear crack
C	(1)	general representation of initial conditions on nucleation source
D_c	(6)	characteristic sliding distance for evolution of fault state
G	(A1)	shear modulus
H	(7),(A8)	term containing model parameters for nucleation source
k	(7),(A1)	effective stiffness of nucleation source
l	(A1)	dimension fault patch
l_c	(A2)	characteristic dimension of nucleation source
n	(2)	earthquake sequence number indicating n th source in distribution.
m	(B20)	term used in solution for stressing by logarithm of time
r	(2)	reference seismicity rate
R	(11),(B24)	seismicity rate
R_0	(16)	seismicity rate immediately following a stress step
t	(1)	time, time of instability
t_a	(12)	characteristic time for seismicity to return to steady state
t_e	(18)	characteristic time for initiation of aftershock decay
t_r	(19)	mean earthquake recurrence time
u, w	(B18)	parameters for characterization of stressing by the logarithm of time
x	(20)	distance from center of center of shear crack
α	(6)	constitutive parameter for evolution of state with normal stress
γ	(7)	state variable for seismicity formulation
γ_{ss}	(10)	steady state value of γ
$\delta, \dot{\delta}$	(5)	slip and slip speed
η	(A1)	crack geometry parameter
μ_0	(5)	nominal coefficient of friction
θ	(5)	state variable in fault constitutive formulation
σ	(5)	normal stress
$\tau, \dot{\tau}$	(1)	shear stress and shear stressing rate
$\dot{\tau}_r$	(3)	reference stressing rate
$\Delta\tau_e$	(19)	earthquake stress change (negative)
ξ	(A2)	scaling parameter for critical fault length l_c for unstable slip

applications may require numerical treatment (for example, by time-marching, using steps composed of simple stressing functions). In order to update initial conditions for each time step, such applications require determination of the change of C arising from the stressing history and the nucleation process.

As formulated, this approach does not predict the specific magnitude of individual earthquakes within the magnitude range that is implicit in the definition of r . However, because the formulation yields rate of production of earthquakes in response to a stressing history, it can be combined with magnitude-frequency relations or may be used in conjunction with stochastic models that employ seismicity rate.

Implementation using rate- and state-dependent friction. Using solutions for the nucleation of slip instabilities on faults with rate- and state-dependent fault strength [Dieterich, 1992] the procedure just presented is followed to obtain a specific formulation for rate of earthquake production. In Appendix A derivations for the nucleation process have been generalized somewhat from Dieterich [1992]. In Appendix B the distributions of initial conditions and earthquake times corresponding to equations (3) and (4), respectively, are derived. On the basis of these results a general formulation for rate of earthquake production is obtained. Results of those derivations are summarized below.

The rate- and state-dependent representation of fault constitutive properties provides a framework to quantify somewhat complicated experimental observations of fault properties and to unify concepts of dynamic/static friction, earthquake fracture energy, displacement weakening, time-dependent healing, slip history dependence and slip speed dependence [Dieterich, 1979a, 1981; Ruina, 1983]. In addition to representing observed transient and steady state velocity dependencies during stable sliding, this constitutive relation has been applied to model the spontaneous time-dependent onset of unstable slip in laboratory experiments [Dieterich, 1979b, 1981; Ruina, 1983; Rice and Gu, 1983; Weeks and Tullis, 1985; Blanpied and Tullis, 1986; Okubo and Dieterich, 1986; Tullis and Weeks, 1986], fault creep [Scholz, 1988], earthquake afterslip [Marone et al., 1991] and the earthquake cycle along plate boundaries [Tse and Rice, 1986; Stuart, 1988].

Several essentially equivalent rate- and state-dependent fault constitutive representations have been discussed in the literature. A simplified form used by Ruina [1983], based on Dieterich [1979a, 1981], and generalized for multiple state variables [Rice and Gu, 1983] may be written as

$$\tau = \sigma \left[\mu_0 + A \ln\left(\frac{\dot{\delta}}{\dot{\delta}^*}\right) + B_1 \ln\left(\frac{\theta_1}{\theta_1^*}\right) + B_2 \ln\left(\frac{\theta_2}{\theta_2^*}\right) + \dots \right], \quad (5)$$

where τ and σ are shear and normal stress respectively, $\dot{\delta}$ is slip speed, and θ_i are state variables. Parameters μ_0 , A , and B_i are experimentally determined coefficients. The terms with asterisks are normalizing constants.

Applications to problems in nature have generally employed only one state variable. Simulations of some laboratory experiments has been improved by use of two

state variables [Ruina, 1983; Weeks and Tullis, 1985; Tullis and Weeks, 1986]. Because little complexity is added, derivation of solutions for the nucleation process (Appendix A) and derivations pertaining to earthquake rates with populations of sources (Appendix B) retain the use of multiple state variables.

From experimental observations, state is inferred to depend on sliding and normal stress history. This study employs

$$d\theta_i = \left[\frac{1}{\dot{\delta}} - \frac{\theta_i}{D_{c_i}} \right] d\delta - \left[\frac{\alpha_i \theta_i}{B_i \sigma} \right] d\sigma \quad (6)$$

for evolution of state by displacement δ and normal stress σ . In (6), D_{c_i} is a characteristic displacement and α_i is a parameter governing normal stress dependence of θ_i . At steady state ($\sigma = \text{const}$, $d\theta/dt = 0$) $\theta_{ss} = D_c/\dot{\delta}$. When not at steady state, θ seeks θ_{ss} over the sliding distance D_c . The displacement dependence of (6) is that proposed by Ruina [1983], and the normal stress dependence is from Linker and Dieterich [1992]. An alternate representation of displacement dependence of θ , used in several studies [e.g., Tse and Rice, 1986; Tullis and Weeks, 1986], does not permit the simple derivations employed here, but numerical simulations of the nucleation process give comparable results for the time dependence of earthquake nucleation for both evolution laws [Dieterich, 1992].

The nucleation process on faults with these properties is characterized by an interval of self-driven accelerating slip that precedes instability. Over a range of stresses the logarithm of the time to instability is found to increase with decreasing stress. Simulations of faults with heterogeneous properties show that (1) the zone of most rapid acceleration tends to shrink to a characteristic fault length l_c (Appendix A, equation (A2)) as the time of instability approaches and (2) nucleation sources of length l_c develop spontaneously in regions where the shear stress relative to the sliding resistance averaged over l_c is higher than the surroundings. In the context of the current model the population of sources is postulated to arise from heterogeneity of fault conditions.

In general, slip speed is determined by the independent variables θ , τ , and σ . It is shown in Appendix A that in an accelerating slip patch evolution of θ is determined by slip. Under this condition the dependence of the time to instability on initial conditions is fully specified by the initial slip speed $\dot{\delta}_0$ of the patch (Appendix A, equation (A7)). Slip speeds remain very small until a short time prior to the onset of instability. Hence the interval of premonitory slip may be quite long.

Following the procedure described above, the distribution of initial slip speeds from Appendix B is

$$\dot{\delta}(n) = \frac{1}{H\sigma\gamma \left[\exp\left(\frac{i_r n}{A\sigma\tau}\right) - 1 \right]}, \quad (7)$$

where $H = (B/D_c) - (k/\sigma)$; k is the effective fault patch stiffness and γ is a state variable that evolves with time and stressing history. The term H does not appear again in the formulation. For the initial reference distribution corresponding to (3), γ takes the value

$$\gamma = \frac{1}{\dot{\tau}_r} \quad (8)$$

Because slip speed increases as the nucleation process develops, the distribution of slip speeds evolves with time. Appendix B shows that the distribution retains the form of (7), independent of subsequent stressing history, but γ evolves with stressing history as described by

$$d\gamma = \frac{1}{A \sigma} \left[dt - \gamma d\tau + \gamma \left(\frac{\tau}{\sigma} - \alpha \right) d\sigma \right] , \quad (9)$$

where $\alpha = \alpha_1 + \alpha_2 + \dots$ for applications involving multiple state variables. Recall that σ is taken to be effective normal stress; hence (9) may be employed to model effects of pore-fluid pressure changes on seismicity rates.

For positive shear stressing rates with $\dot{\sigma} = 0$, equation (9) has the property that γ seeks the steady state value,

$$\gamma_{ss} = 1/\dot{\tau} \quad (10)$$

with the characteristic relaxation time of $(A\sigma/\dot{\tau})$.

The distribution of earthquake times is obtained by substituting the distribution of initial conditions into the solutions for time to instability. In turn, seismicity rate R is obtained by differentiating the distribution of times giving the general result

$$R = \frac{r}{\gamma \dot{\tau}_r} , \quad (11)$$

where r is the steady state seismicity rate at the reference shear stressing rate $\dot{\tau}_r$. From (10) and (11) it is seen that at steady state the ratio of seismicity rates (R/r) is simply $(\dot{\tau}/\dot{\tau}_r)$. Rate R may be interpreted as a statistical representation of expected rate of earthquake production for some magnitude interval.

Equations (9) and (11) are a principal result of this study and represent a state-dependent constitutive formulation for rate of earthquake production. Some useful nonsteady state solutions of (9) are given in Appendix B. These include evolution of γ with time under constant stress, linear change of shear stress with time, and change of shear stress with the logarithm of time (equations (B7), (B17), and (B21), respectively) and evolution of γ for step of shear and normal stress (equation (B11)).

Figure 1 plots the slip speed distribution of equation (7) against instability time. Also shown is the effect of a stress step on the distribution as given by (B11).

Effects of simple stressing perturbations on seismicity rate may be obtained by substituting solutions of (9) into (11) assuming the seismicity is initially at steady state ($\gamma_0 = 1/\dot{\tau}_r$). For simulation of complex stressing histories a straightforward procedure consists of breaking the stressing history into time steps of constant shear stressing rate and stress steps (of τ and σ) and successively applying the appropriate solutions to follow the evolution of γ from increment to increment. Seismicity during a time step is then obtained by substituting the result for evolution of γ with time ((B7) or (B17)) into (11). Alternatively, numerical solutions of (9) may be obtained.

Parameter values. To implement the model, fault constitutive parameters A and α which appear in (9) and (11) must be specified. From laboratory observations, coefficient A generally has values in the range 0.005 to 0.012 for various temperature and pressure conditions. Under hydrothermal conditions, it appears that somewhat larger values ($A \sim 0.02$) may be appropriate [Blanpied et al., 1991;

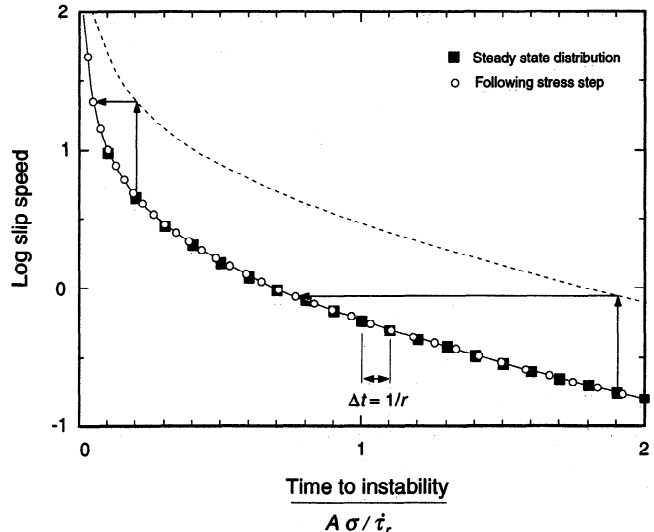


Figure 1. Distribution of slip speeds against time to instability. The solid curve is the solution for time to instability given an initial slip speed of the nucleation source (equation (A11) of Appendix A). Solid squares give the distribution of slip speeds from equation (7) under the reference condition at constant seismicity rate r . Small circles show the effect of a stress step on the distribution from solution of evolution equation (9). This solution is given in Appendix B (equation (B11)). The effect of a stress step is to increase slip speed (vertical arrows) of each source as given by (A17). This increase of slip speed decreases the time to instability (horizontal arrows) and results in higher density of points (higher seismicity rate) at short times but does not affect density at larger times where the dependence of time to instability against log slip speed is linear. Hence with the passage of time, the perturbation of seismicity rates from the stress step evolves out of the system.

M. L. Blanpied, personal communication, 1992]. Numerical examples in the following use $A = 0.01$. Experimental determination of α is presently limited to a single study [Linker and Dieterich, 1992] which obtained $\alpha = 0.23$ and established generally that $0 \leq \alpha \leq \mu_{ss}$, where μ_{ss} is steady state sliding friction.

Application to Earthquake Clustering

Seismicity rate following a stress step. To illustrate and test the model some characteristics of rate of earthquake production following a stress step have been explored. It is proposed that several types of clustered earthquake phenomena represent a perturbation of background seismicity resulting from the change of stress state caused by previous earthquakes.

In the interest of simplicity the stress step induced by a previous earthquake on the surrounding region is represented as a positive step in shear stress, $\Delta\tau$, with normal stress held constant. The solution of (9) for a stress step (B11) shows that a decrease of effective normal stress σ produces the same qualitative effect as an increase of shear stress in that both decrease γ and lead to higher rates of earthquake production. Subsequent evolution of γ is independent of prior processes that caused γ to change.

Hence time-dependent features described below that result from a positive step of shear stress would also arise from negative steps of normal stress. The following applications further assume constant $\dot{\tau}$ following a stress step and steady state seismicity rate r before the step (i.e., $\gamma_0 = 1/\dot{\tau}_r$).

Under these assumptions, simple expressions may be obtained for seismicity rate. First, equation (B11) is employed to evolve γ through the stress step to obtain γ immediately after the step. This becomes γ_0 in (B7) or (B17) which then gives the evolution of γ for the subsequent time interval where stressing rate is assumed constant. Finally, the expressions for γ resulting from these operations are substituted into (11) to yield seismicity rate as a function of time after the stress step:

$$R = \frac{r\dot{\tau}/\dot{\tau}_r}{\left[\frac{\dot{\tau}}{\dot{\tau}_r} \exp\left(\frac{-\Delta\tau}{A\sigma}\right) - 1 \right] \exp\left[\frac{-t}{t_a}\right] + 1}, \quad \dot{\tau} \neq 0, \quad (12)$$

and

$$R = \frac{r}{\exp\left(\frac{-\Delta\tau}{A\sigma}\right) + t\dot{\tau}_r/A\sigma}, \quad \dot{\tau} = 0 \quad (13)$$

where $\dot{\tau}_r$ and $\dot{\tau}$ are the stressing rate prior to and following the step, respectively, t is set to zero at the time of the stress step, and

$$t_a = \frac{A\sigma}{\dot{\tau}} \quad (14)$$

is the characteristic relaxation time for the perturbation of earthquake rate. Note that for $\Delta\tau = 0$ and $\dot{\tau} \neq \dot{\tau}_r$ (12) gives the time-dependent change of seismicity for a change of stressing rate from $\dot{\tau}_r$ to $\dot{\tau}$. Figure 1 illustrates equation (12) by showing the effect of a stress step on the distributions of slip speeds and nucleation times.

Origin of aftershocks. It is proposed that aftershocks are caused by the steplike change of stress that occurs at the time of the mainshock. Two general observations support this hypothesis. First, aftershocks often cluster in those areas near a mainshock rupture where stress changes favor aftershock fault slip, including zones off the principal fault plane [e.g., Stein and Lisowski, 1983]. Second, sudden jumps of stress from causes unrelated to fault slip also stimulate aftershocklike bursts of seismicity followed by the $1/t$ decay characteristic of aftershock sequences. An example of the latter are aftershocklike bursts of seismic activity on the south flank of Kilauea volcano following dike intrusion events [Dvorak *et al.*, 1986].

Equations (12) and (13) are plotted in Figure 2. Note that equation (13) has the form of Omori's law for aftershock decay:

$$R = \frac{a}{b + t} \quad (15)$$

Similarly, equation (12) gives Omori's law for $t/t_a < 1$, but seismicity rate merges to the steady state background rate for $t/t_a > 1$. This characteristic of (12) makes it a somewhat preferable representation of aftershock decay for many applications.

The agreement of this model with Omori's law permits assignment of physical interpretations to aftershock parameters. From (13) and (15),

$$\begin{aligned} a &= \left(\frac{A\sigma}{\dot{\tau}_r} \right) r, \\ b &= \left(\frac{A\sigma}{\dot{\tau}_r} \right) \exp\left(\frac{-\Delta\tau}{A\sigma}\right) = \left(\frac{A\sigma}{\dot{\tau}_r} \right) \left(\frac{r}{R_0} \right), \end{aligned} \quad (16)$$

where R_0 is the initial seismicity rate following the step at $t = 0$. If stressing rate is the same before and after the mainshock ($\dot{\tau}_r = \dot{\tau}$), then from (14), $(A\sigma)/\dot{\tau}_r = t_a$ and

$$a = rt_a, b = t_a \exp\left(\frac{-\Delta\tau}{A\sigma}\right) = t_a \left(\frac{r}{R_0} \right). \quad (17)$$

As shown in Figure 2, normalized seismicity rates R/r for different stress steps all decay along the same $1/t$ asymptote. The characteristic time t_e for the rate to merge with the $1/t$ asymptote is obtained by solving for the intersection of R_0 with the asymptote formed by setting $\Delta\tau = \infty$ in (13) giving

$$t_e = \frac{A\sigma}{\dot{\tau}_r} \exp\left(\frac{-\Delta\tau}{A\sigma}\right) = b. \quad (18)$$

See Figure 2 for graphical interpretation of t_e .

Aftershock duration. Aftershock duration is defined here as t_a , the characteristic time for aftershocks to return to the background seismicity rate. From (14), t_a is independent of the magnitude of the stress step but depends upon stressing rate. Assuming the approximate relation $\dot{\tau} = -\Delta\tau_e/\dot{\tau}_r$, where $\Delta\tau_e$ is the stress change on the mainshock rupture, and t_r is mean earthquake recurrence time, gives

$$t_a = \frac{A\sigma}{\dot{\tau}} = t_r \frac{A\sigma}{-\Delta\tau_e}. \quad (19)$$

The negative sign in (19) arises because stress decreases on the earthquake rupture surface. A similar result is given by Dieterich [1988b]. Equation (19) constitutes a specific prediction of this model. In this prediction, earthquake magnitude does not explicitly affect aftershock duration but

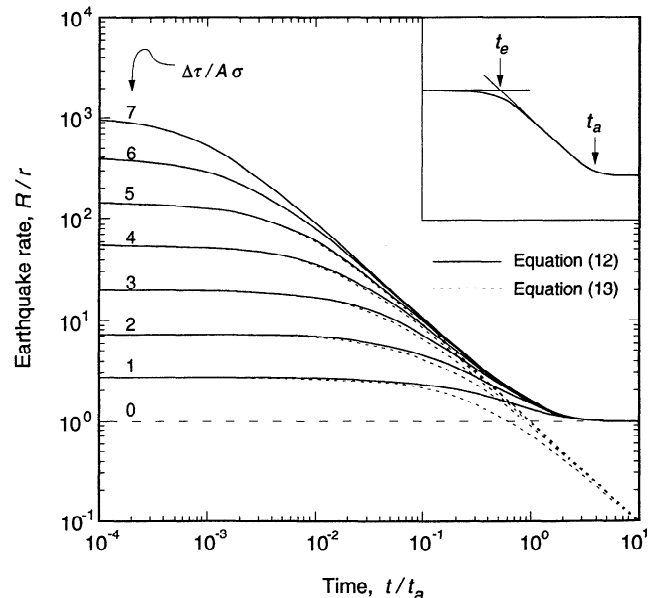


Figure 2. Seismicity rate following a stress step from equations (12) and (13) for the cases $\dot{\tau} \neq 0$ and $\dot{\tau} = 0$, respectively. The family of curves gives solutions for the indicated values of stress step $\Delta\tau$ normalized by $A\sigma$. The inset illustrates the definition of t_e .

will enter indirectly if t_r is a function of magnitude. As a test of this predicted dependence of aftershock duration on recurrence time, some preliminary data for t_a and t_r have been assembled. Data sources and methods of parameter estimation are summarized in Table 2. Figure 3 plots the data and the predicted relationships between recurrence time and aftershock duration. These results, though quite

preliminary and having large scatter, appear consistent with the prediction of (19) and suggest that more systematic study of aftershock duration may be warranted.

Spatial effects due to nonuniform stress changes. Because aftershock rate depends on the magnitude of the stress step, systematic spatial variations of the magnitude of the stress change will result in systematic spatial variation

Table 2. Earthquake Recurrence and Aftershock Duration

Event	Location	Magnitude	t_a , years	t_r , years	Data Sources and Method of Estimation
1	Bear Valley, California, 1972	5.0	0.2-0.5	14-21	Recurrence times are from <i>Ellsworth and Dietz</i> [1990]. Aftershock duration is obtained by fit to aftershock equation (12).
2	Coyote Lake, California, 1979	5.7	1.4-2.5	54-82	Upper limit on recurrence time from <i>Reasenberg and Ellsworth</i> [1982]. Minimum recurrence time is estimated assuming slip of 70 cm and Calaveras fault slip rate of 1.3 cm/yr from <i>Matsu'ura et al.</i> [1986]. Aftershock duration is obtained from fitting of aftershock data [<i>Reasenberg and Ellsworth</i> , 1982] to equation (12).
3	Loma Prieta, California, 1989	7.1	1.7-3.5	84-100	Recurrence time is from <i>Working Group</i> [1990]. Aftershock duration is provided by P. Reasenberg (written communication, 1992).
4	Kalapana, Hawaii, 1975	7.5	8.5-11.2	50-100	Recurrence time is estimated from rift opening rate of 6-12 cm/yr and net offset of 6 m [Dieterich, 1988a]. This is generally consistent with recurrence following the great earthquake of 1868 [Wyss, 1988]. Aftershock duration obtained by fitting aftershock decay to equation (12).
5	Koaiiki, Hawaii, 1983	6.7	1-1.7	10.5-21	Recurrence time is from Wyss [1986]. Aftershock duration is obtained by fitting aftershock decay to equation (12).
6	Alaska, 1964	9.2	4.6-9.6	230-615	Recurrence time is estimated assuming plate slip rate of 6.5 cm/yr and earthquake slip of 15-40 m. Aftershock duration is from data supplied by J. Lahr (personal communication, 1990).
7	Nobi, Japan, 1891	~8	≥ 78	5,000-20,000	Recurrence time from <i>Tsukuda</i> [1983] is based on dating of paleoseismic events. Aftershocks of this event continue to at least 1969 without showing any indication of returning to a background rate [<i>Utsu</i> , 1969].
8	Rat Islands, Alaska, 1965	8.7	2.7-5.5	72-120	Aftershock duration is obtained by fitting of data from <i>Ogata and Shimazaki</i> [1984] to equation (14). Recurrence time is estimated assuming plate motion rate of 8.3 cm/yr and earthquake slip of 6-10 m.
9	San Francisco, California, 1906	8	5-10	129-281	Recurrence time is taken to be range of estimates for recurrence on San Francisco peninsula and North Coast segments from <i>Working Group</i> [1990]. Aftershock duration is from data of <i>Ellsworth et al.</i> [1981].
10	San Juan Bautista, California, 1979	4.8	0.5-0.8	4-8	Recurrence time is estimated from fault slip rate of 2.5 cm/yr [<i>Matsu'ura et al.</i> 1986] and estimated slip of 10-20 cm. Aftershock duration is obtained by fitting of aftershocks to equation (12).

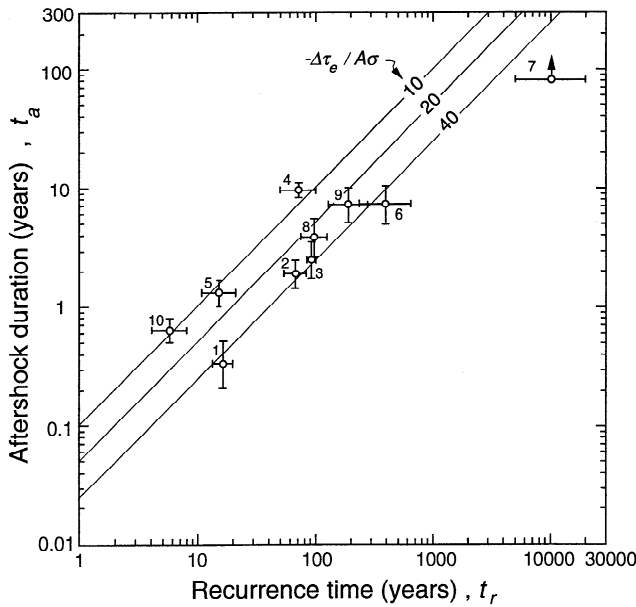


Figure 3. Observed and predicted aftershock duration t_a against mainshock recurrence time t_r . Curves give solutions of equation (19) for indicated values of mainshock stress drop $\Delta\tau_e$ normalized by $A\sigma$. Sources of data are summarized in Table 2.

of seismicity in the vicinity of a previous earthquake. The following gives a simplified representation of stress change from slip on a planar surface in a homogeneous elastic medium which should be common to all earthquakes:

$$\Delta\tau = -\Delta\tau_e \left[\left(1 - \frac{c^3}{x^3} \right)^{-1/2} - 1 \right], \quad x > c \quad (20)$$

where c is crack radius and x is radial distance from the center of the crack. This approximation does not represent azimuthal dependencies of shear stress, but it does incorporate both the square root stress singularity at the crack tip and the stress falloff by $1/x^3$ at larger distances which are characteristic of cracks in an elastic medium. Equation (20) is employed to illustrate general characteristics of seismicity resulting from a nonuniform stress change in the vicinity of an earthquake rupture. Other stress components and stresses at locations not lying on the projection of the mainshock fault surface will show comparable distance effects. However, application of the model to specific aftershock patterns would of course require detailed computation of the entire stress field.

Substitution of (20) into (12) gives seismicity rate as a function of time and distance following a uniform stress change $\Delta\tau_e$ on a circular crack:

$$R = \frac{r\dot{\tau}/\dot{\tau}_r}{\left\{ \frac{\dot{\tau}}{\dot{\tau}_r} \exp \left[\left(\frac{\Delta\tau_e}{A\sigma} \right) \left(\left\{ 1 - \frac{c^3}{x^3} \right\}^{-1/2} - 1 \right) \right] - 1 \right\} \exp \left[\frac{-t}{t_a} \right] + 1}, \quad x > c, \dot{\tau} \neq 0. \quad (21)$$

Using (19), the term $\Delta\tau_e/A\sigma$ appearing in (21) may be replaced by $-t_r/t_a$. Figure 4 shows rate as a function of distance at different times using (21).

The net seismicity rate originating from a finite region surrounding a mainshock may be obtained by numerically integrating (21) over the region of interest. Figure 5 gives results for finite regions assuming r , $\dot{\tau}/\dot{\tau}_r$, and $A\sigma$ are the same everywhere. For a finite region it is found that earthquake rate R decays by $(1/t)^p$, where $p = \sim 0.8$. This is in contrast to the decay by $1/t$ arising at any point or for finite regions where the stress change is uniform. The decrease of decay rate derives from the dependence of t_a on magnitude of the stress step. At time t some regions will be at $t < t_e$ (rate approaches constant rate asymptote) while other regions will be at $t > t_e$ (rate decays along the $1/t$ asymptote).

Figure 5 also illustrates a potential source of bias that can arise in estimation of aftershock parameters such as t_a where aftershock rates vary in space. Estimates of aftershock duration may be seriously underestimated if regions with little or no increase in earthquake rate are included in the aftershock count. For example, in Figure 5 the cumulative rate over the region from $x/c = 1.001$ to the large, essentially unperturbed distance of $x/c = 8$ also shows an interval of decay with $p \sim 0.8$ but has an apparent aftershock duration that is much less than the actual duration.

Aftershock zones characteristically expand with time [Tajima and Kanamori, 1985; Wesson, 1987]. Apparent spread of an aftershock zone in the present model arises from the nonuniform stress change of the mainshock. Substituting the expression for $\Delta\tau$ of (20) into (18) yields

$$t_e = t_a \exp \left[\frac{\Delta\tau_e}{A\sigma} \left(\left\{ 1 - \frac{c^3}{x_e^3} \right\}^{-1/2} - 1 \right) \right], \quad x > c, \quad t_e \leq t_a. \quad (22)$$

Again, the result of (19) may be used to replace the $(\Delta\tau_e/\sigma A)$ term. Recall that t_e is the characteristic time that the aftershock rate begins to merge with the $1/t$ asymptote.

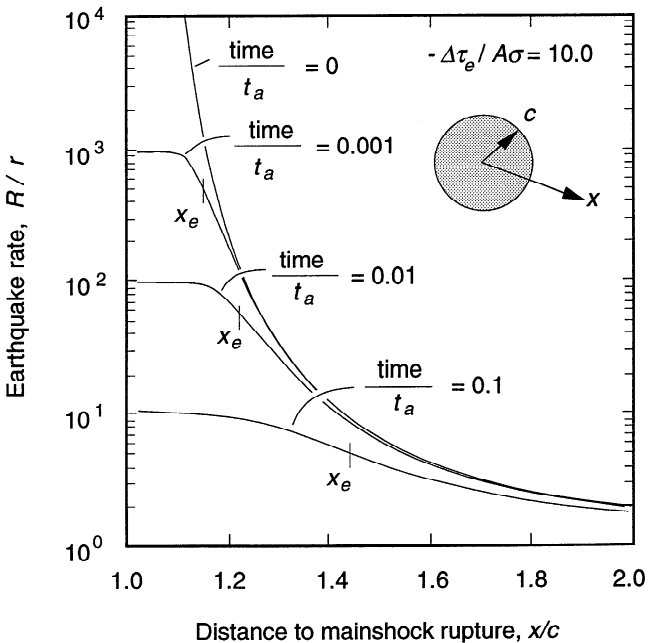


Figure 4. Earthquake rate from equation (21) against distance at different times following a prior earthquake. The points labeled x_e indicate the apparent edge of the aftershock zone as given by equation (22).

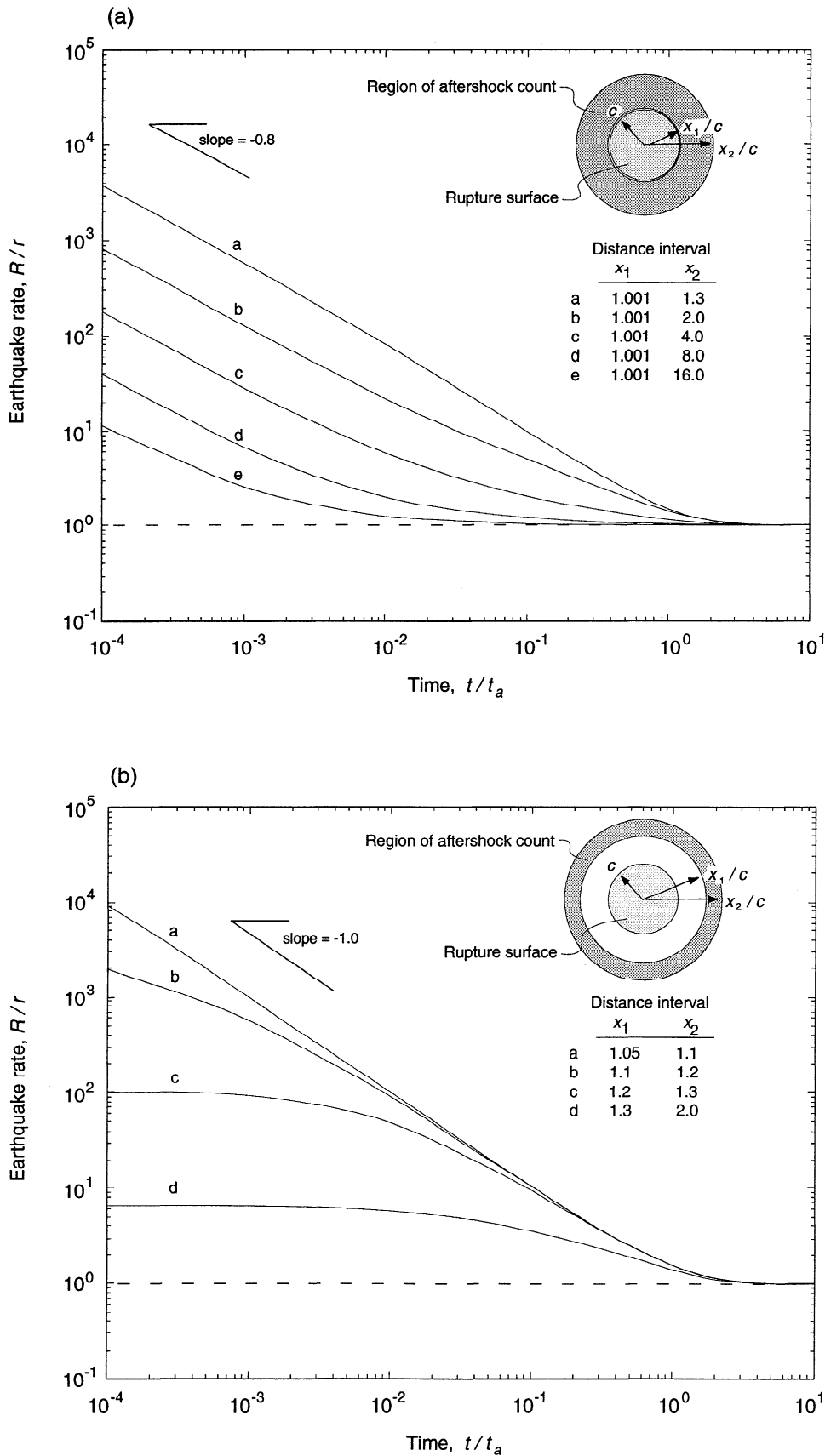


Figure 5. Predicted net aftershock rate for finite regions surrounding a shear crack (see equation (21)). (a) Seismicity rate for cumulative distance from edge of crack. (b) Seismicity rate for annular distance segments.

At distance $\leq x_e$ normalized rates R/r begin to approach the same $1/t$ asymptote and become independent of the original stress change. However, at $x > x_e$, the normalized rates are smaller and scale by $\exp(\Delta\tau/A\sigma)$, where $\Delta\tau$ decreases with distance. Hence x_e in (22) marks the location of the apparent edge of the aftershock zone at time t_e . As $x_e \rightarrow \infty, t_e \rightarrow t_a$, and aftershocks merge with the background rate.

The position of x_e at successive time steps is indicated in the example of Figure 4. Figure 6 shows the position of x_e against t_e from (22). The expansion curves of Figure 6 appear to be generally consistent with the aftershock observations of Tajima and Kanamori [1985] and Wesson [1987] for values of (t_r/t_a) in the range 10 to 50 which are also suggested by the data of Figure 3. The predicted smooth expansion of the aftershock region shown in Figure 6 assumes both idealized stress changes of (20) and that parameters r , A , and σ do not vary with location. Less systematic propagation of aftershock zones will occur if the restrictions of these assumptions are relaxed.

Nonconstant stressing following an earthquake.

Figure 7 illustrates seismicity for a sequence of stress steps representing a hypothetical stressing history consisting of a mainshock followed by two large aftershocks. This example assumes uniform stress changes over the region of interest and follows the evolution of γ through the several loading ramps and steps by successive application of (B17) and (B11), respectively. Following each stress step, t is set to zero and the value of γ at the end of the stress step becomes γ_0 for the next loading ramp. Note, that the calculated seismicity rate, when plotted against the logarithm of the time following the mainshock, gives the appearance that the durations of secondary aftershock sequences scale by the time following the mainshock. Note also that the effect of secondary aftershocks is to increase the slope of the aftershock decay. Both effects are artifacts of plotting the entire sequence against logarithm of time after the mainshock. If rates are plotted against logarithm of time following each later stress step, the slope of the decay

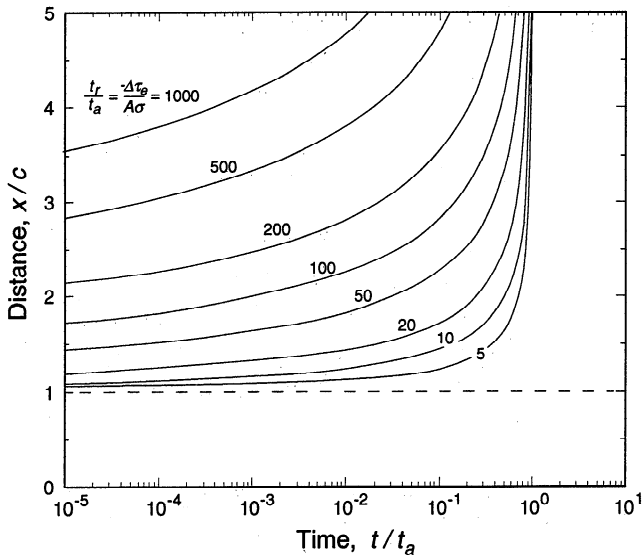


Figure 6. Expansion of aftershock zone from equation (22). Curves give the position of the edge of the aftershock zone x_e for the indicated values of the mainshock stress drop $\Delta\tau_r$ normalized by $A\sigma$.

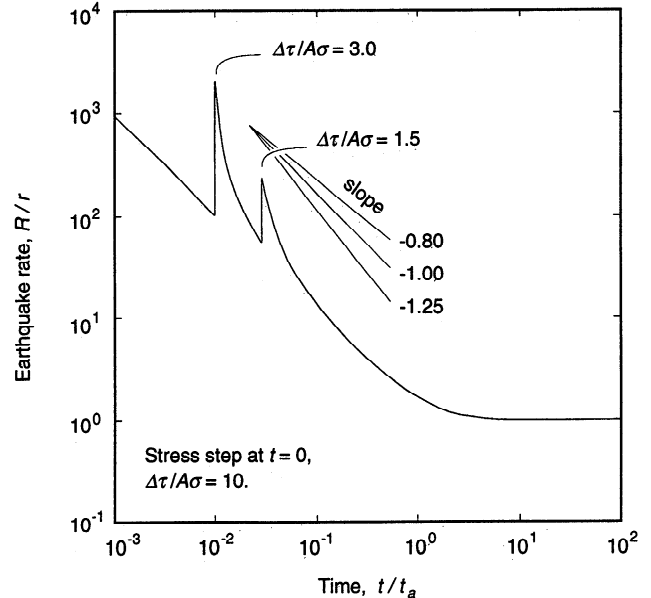


Figure 7. Seismicity rate for stressing history consisting of several stress steps. The second and third stress steps represent large aftershocks which give rise to secondary aftershock sequences.

following the step again gives $p = 1$ with characteristic time of decay t_a .

In general, nonconstant stressing history following an earthquake stress step may alter aftershock decay rates. Figure 8 gives earthquake rate for a stressing history consisting of an initial stress step at $t = 0$ followed by stressing that varies with the logarithm of time. Evolution of γ was found by first applying equation (B11) for a stress step then applying equation (B21) for stressing by logarithm of time. This example provides an illustration of effects that would arise from creep processes that add to, or relax, an earthquake stress step. If stress increases with the logarithm of time, the slope of the aftershock decay again gives $p = 1$. Note, however, that such loading can produce an initial buildup of earthquake rates prior to decay. If stress decreases by logarithm of time, rapid decay with $p > 1$ is possible.

Earthquake clustering. Aftershocks are but one manifestation of the pronounced tendency of earthquakes to cluster in space and time. In their study of earthquake clustering, Kagan and Jackson [1991] first assembled data from several earthquake catalogs giving the space and time statistics on the occurrence of earthquake pairs above some magnitude threshold. These data appear to provide a comprehensive and robust characterization of earthquake clustering which is well suited for a test of the present model. The following test is based on the Kagan and Jackson plots of all earthquake pairs (i.e., before they applied the declustering algorithms used in their subsequent analysis) and therefore includes independent events, foreshocks, aftershocks, and other possible types of clustered events.

Data (prior to declustering) for shallow earthquakes derived from the Harvard catalog and for intermediate and deep earthquakes from the PDE catalogues are reproduced from Kagan and Jackson [1991] in Figures 9a, 9b, and 9c, respectively. These data give observed numbers of earthquake pairs normalized by the expected number

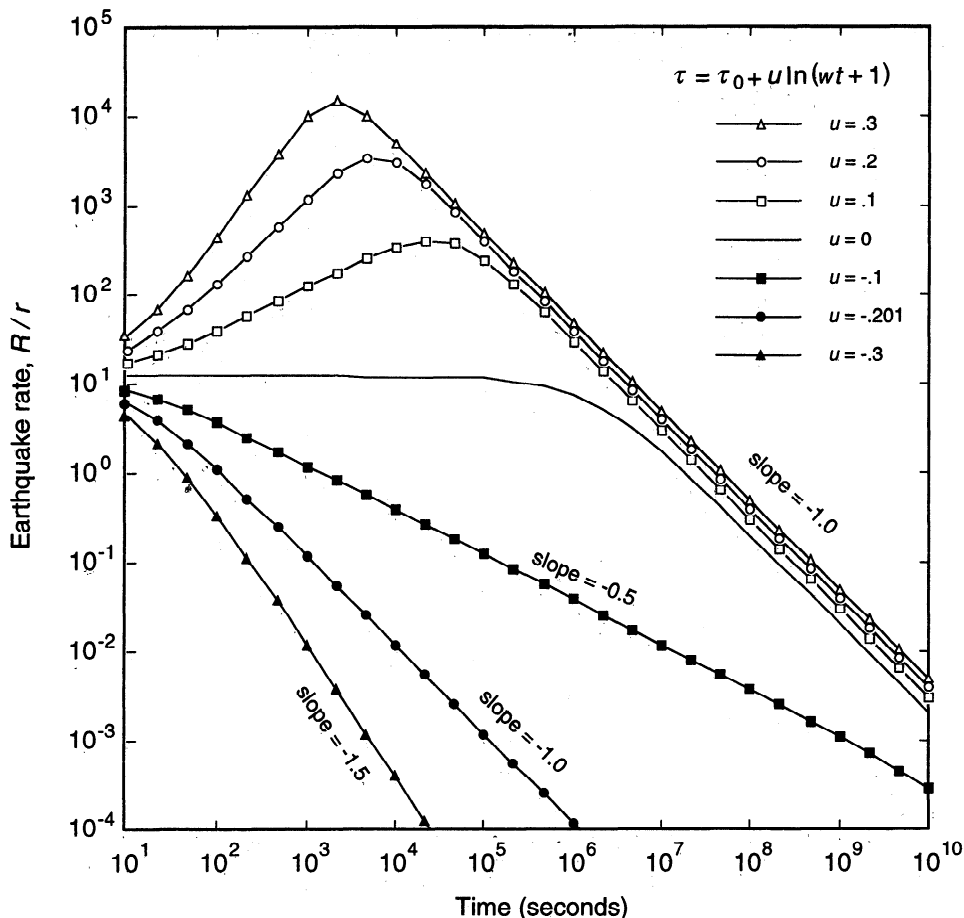


Figure 8. Seismicity rate for a stressing history composed of a stress step followed by change of stress with logarithm of time. Parameters for the computation are $A = 0.01$ MPa, $\sigma = 20$ MPa, $\Delta\tau = 0.5$ MPa, and $w = 10$ s. If stress increases with the logarithm of time, seismic activity first increases then decays by $1/t$. If stress decreases with the logarithm of time, seismic activity decays by rates that can exceed the $1/t$ decay.

assuming Poisson occurrence. The normalized number of pairs are computed for cumulative time and cumulative distances from the first event of all possible pairs. Each data set shows significant clustering of earthquakes characterized by an interval in which normalized frequency decays with time by $(1/t)^p$ with $p \sim 0.8$. Below, it is found that apparent clustering to the very great distances shown in Figure 9 arises as a consequence of the convention of using cumulative distance intervals instead of differential intervals for the summing of earthquake pairs.

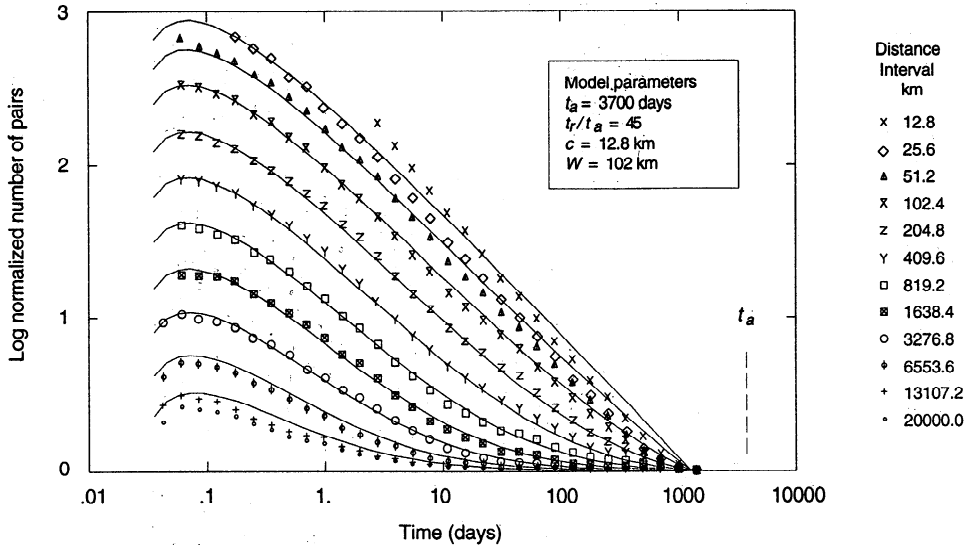
Simulation of these data with the present model assumes the rate of occurrence of the second earthquake of all possible pairs is perturbed by the stress step of the previous earthquake as given by (21). Because the stress as given by (20) is singular at $x = c$, for this application (21) has been modified to limit the stress increase to a maximum value of $-\Delta\tau_e$. The simulations employ an idealized geometry of a seismogenic belt (Figure 10) which is represented as a surface of half width W . The analysis assumes that before the first earthquake of any pair, the unperturbed background rate of seismicity is the same everywhere along the surface. The first earthquake in the pair has a radius c and is assumed to occur in the middle of the belt. Numerical integration of the modified version of equation (21) gives the cumulative number of earthquake pairs to time t from

the first event and over the distance interval from $x = c$ to $x = 2c, 4c, 8c$, etc. Because the Kagan and Jackson analysis began the count of pairs only after some finite interval of time had elapsed following the first event, the integration for the simulations also began at finite elapsed time t_0 . To obtain the model statistic equivalent to Kagan and Jackson, the net number of events cumulative to each time and distance was then normalized by the expected number assuming there was no interaction. All simulations assume that the stressing rate before and after the first event are the same.

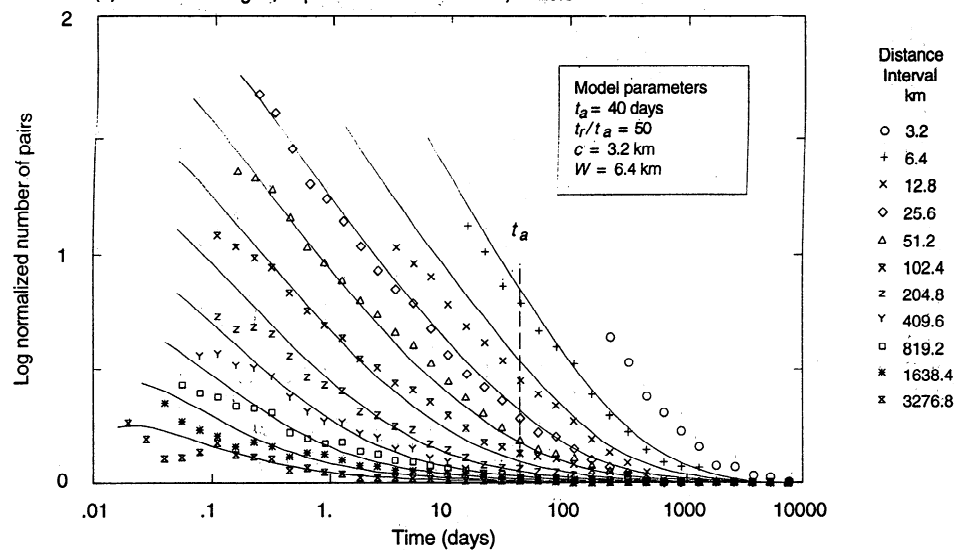
Results of simulations are plotted in Figure 9. Parameters for the simulations $t_a, \Delta\tau_e/A\sigma = t_r/t_a$, and W were determined by trial and error to fit the data and are listed in Table 3. To reduce the number of free variables, c was fixed as the minimum distance employed by Kagan and Jackson which was judged to represent a reasonable approximation of the source radius of the mean catalogue magnitude. The simulations are only moderately sensitive to model parameters in that nearly as good fit to the data could be achieved with somewhat different parameter values (see Table 3).

The stress-step solution appears to provide a rather good representation of the data including intermediate and deep earthquakes which may involve mechanical processes that

Data from Kagan and Jackson (1991)
 (a) HARVARD catalogue, depth interval 0 - 70 km, $M \geq 6.0$



Data from Kagan and Jackson (1991)
 (b) PDE catalogue, depth interval 71 - 280 km, $M \geq 5.3$



Data from Kagan and Jackson (1991)
 (c) PDE catalogue, depth interval 281 - 700 km, $M \geq 5.3$

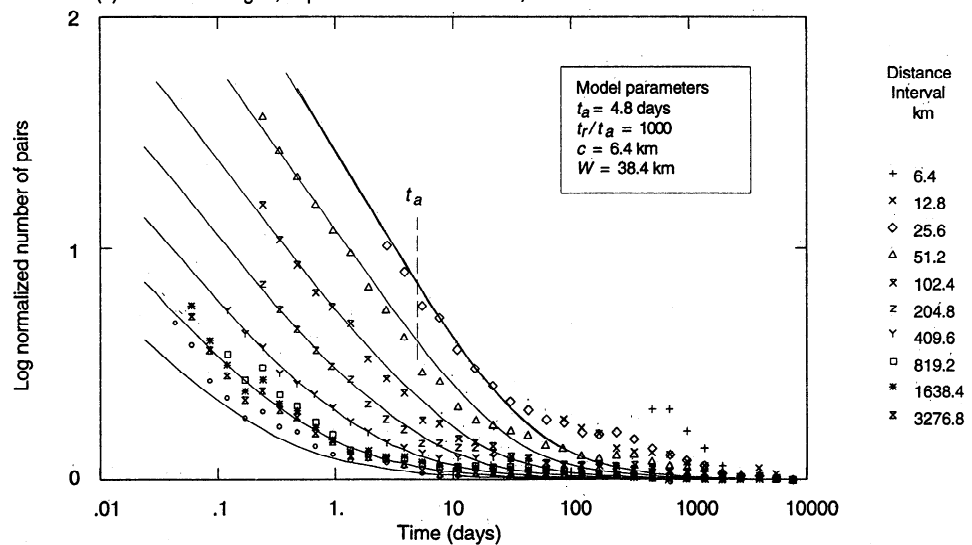


Figure 9. Clustering of earthquake pairs for (a) shallow, (b) intermediate, and (c) deep earthquakes. Data are from Kagan and Jackson [1991]. Curves give examples of simulations using the model of Figure 10.

Table 3. Range of Parameters Giving Satisfactory Fit to Data of Figure 9

Catalog	Depth	Magnitude	Data		t_r/t_a	Source
			t_a , years	$(-\Delta t_e/A\sigma)$		
Harvard,	0–70 km,	$M \geq 6.0$	10.2*	45*	12.8*	102.0*
			10.2	75	12.8	179.0
			10.2	25	12.8	57.8
PDE,	71–280 km,	$M \geq 5.3$	0.11*	50*	3.2*	6.4*
			0.07	150	3.2	12.8
			0.17	25	3.2	3.5
PDE,	281–700 km,	$M \geq 5.3$	0.013*	1000*	6.4*	38.4*
			0.012	3000	6.4	38.4

*Preferred values.

are significantly different from the shallow earthquakes. In each of the examples of Figure 9 the simulations agree to within 10% of the data values for greater than 80% of the data points. The maximum deviations of the simulations from the data are about 50% of a data value. No attempt was made to model the data lying within the source radius of the first event because equation (21) applies to regions outside of the primary rupture area. Seismicity falling within the source region of a prior earthquake is discussed in a later section. For the shallow earthquake data, the results for W appear reasonably consistent with seismogenic zone width. Also, for shallow earthquakes the estimates of t_a and t_r/t_a are consistent with the estimates of Figure 2 and Table 2. However, significantly different values of t_a , t_r/t_a and W are obtained for the intermediate and deep earthquake data. In particular, t_a appears to systematically decrease with increasing depth.

The characteristic shape of the data curves for variation of number of pairs with time is controlled by the stress sensitivity of earthquake rate to elastic stress changes near the first event. The apparent persistence of clustering to the great distances shown in Figure 9 is wholly an artifact of summing the number of pairs cumulatively to some distance x . Highly perturbed seismicity close to the first event is lumped with essentially unperturbed seismicity at greater distances. Comparable effects are seen in the results for net aftershock rate by cumulative distance (Figure 5). As previously discussed for aftershocks, the decay of the normalized number of pairs by $(1/t)^p$ with $p \sim 0.8$ derives from the characteristic stress change surrounding a shear rupture in conjunction with the time and stress dependence of seismicity rate of equation (12). The peaking of number

of pairs at finite times following the first event, with fewer events at shorter times, is also seen in the simulations and arises because the count of earthquake pairs began following some finite time after the first event.

Foreshocks. Foreshock statistics appear very similar to that of aftershocks and to the clustering data discussed above. Histograms of the frequency of foreshock-mainshock pairs show rapid falloff of frequency of pairs with time and distance [Jones and Molnar, 1979; Jones, 1984; Jones, 1985]. For earthquakes in southern California Jones [1985] finds that the probability of a mainshock following a $M \geq 3.0$ earthquake decays by about $(1/t)^p$ with $p \sim 0.9$ which is consistent with the result $p = 0.8$ found for a finite region (Figure 5). In addition, Jones [1985] shows that relative to foreshock magnitude, mainshock magnitudes follow a normal b value distribution down to the size of the foreshock. In the context of the model presented here, the occurrence of mainshock following a foreshock is also interpreted as a perturbation of background seismicity by the stress change of the foreshock as represented equation (21).

Discussion and Conclusions

The approach presented here models seismicity as a sequence of earthquake nucleation events. The distribution of initial conditions over the population of nucleation sources and stressing history determine the timing of events in the sequence. If the nucleation process is assumed to be instantaneous at a critical stress, then rate of earthquake occurrence obtained from this model is simply proportional to stressing rate (assuming monotonic increase of stress). However, the model has been implemented for time-dependent earthquake nucleation. This yields

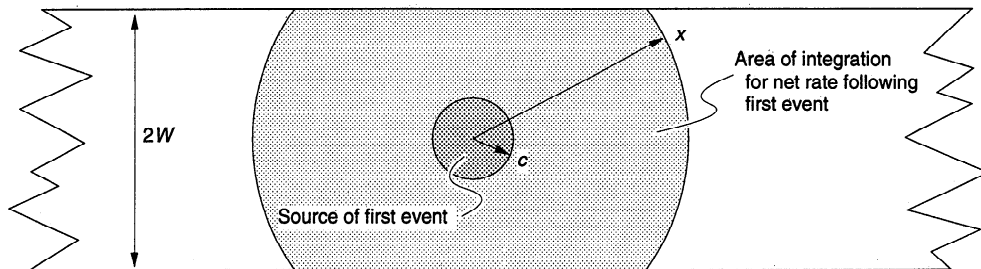


Figure 10. Model employed for simulation of clustering of earthquake pairs. The downdip width of the seismic belt is W . Source radius of the first event is c .

a state-variable constitutive formulation for earthquake rate (equations (9)–(11)) where state depends on stressing history. It is found that seismicity rate seeks a steady state value that is proportional to the instantaneous stressing rate over the characteristic time t_a . An important consequence of this history dependence is that relatively modest jumps in stress result in very large perturbations of earthquake activity as shown, for example, by Figure 3.

Clustered earthquake phenomena have been modeled assuming earthquake rate is perturbed by the elastic stress change associated with prior earthquakes. The model (equations (12) and (13)) yields Omori's law, and in combination with the characteristic elastic stress change in the vicinity of a shear rupture it reproduces the time and distance statistics of earthquake pairs. These results suggest that the formulation contains a reasonable representation of time dependence and stress sensitivity of the earthquake nucleation processes in nature. Because deep earthquakes appear to cluster in a way that is simulated by the present model, but may involve nucleation processes very different from shallow earthquakes [Kirby *et al.*, 1991], more than one time-dependent nucleation mechanism may yield similar results. In particular, if the various types of clustering considered here are driven by characteristic elastic stress changes in the vicinity of an earthquake, then an essential nucleation characteristic needed to model the clustering data is a dependence of the time to instability on an exponential function of the stress change (i.e., $t \propto \exp[(\text{const})(\tau)]$). This is the sensitivity of the time to instability to stress obtained from equations (A13) and (A14) when the relation of initial slip speed to stress is used (equation (A7)).

It is also possible that alternative models of earthquake occurrence might be found that satisfy the various clustering data and do not involve time-dependent nucleation (e.g., viscoelastic or poro-elastic stress transfer following a mainshock). Time-dependent nucleation is a direct consequence of rate and state dependence of fault constitutive properties. To the extent that those properties exist on faults in nature, the nucleation process will be time dependent. An independent argument for the time-dependent nucleation model used here is based on corroboration of these constitutive properties in other applications. There is considerable experimental evidence indicating these properties are characteristic of sliding surfaces in nonmetallic materials including laboratory faults with or without gouge layers. Additionally, various other studies [Tse and Rice, 1986; Scholz, 1988; Stuart, 1988; Okubo, 1989; Marone *et al.*, 1991] have shown that this constitutive representation is effective in modeling fault creep, earthquake afterslip, and various earthquake processes.

An outcome of the approach presented here is that parameters describing clustered phenomena have physical interpretations. For example, a predicted relationship between aftershock duration and stressing rate or recurrence time (equation (19)) has been obtained. In Figure 3 the curves passing through the data for aftershock duration and recurrence time give $t_r/t_a = -\Delta\tau_e/A\sigma = 10\text{--}40$. Similar values ($t_r/t_a = 25\text{--}75$) were obtained with the models of the data for shallow earthquake pairs. Assuming average earthquake stress drops $-\Delta\tau_e = 2.5$ MPa, with $A = 0.01$ and $\Delta\tau_e/A\sigma = 25$, these results suggest a rather low effective normal stress of about 10 MPa. However, this

estimate should probably be viewed with some caution until greater experience with this modeling approach is acquired.

Clustering of intermediate and deep earthquakes have been modeled. The direct relevance of the constitutive formulation to intermediate and deep earthquakes may be questioned, since mechanical processes and earthquake instability mechanisms at those depths may be quite different from those represented by the nucleation model. Nonetheless, the simulations appear to provide a rather good representation of the limited intermediate (70–280 km) and deep (281–700 km) earthquake pair data presented by Kagan and Jackson [1991]. From those simulations (Table 3) it is evident that t_a decreases with depth. This is generally consistent with observations that deep earthquakes have fewer aftershocks [Frolich, 1987]. Also the simulations clearly indicate that, compared to shallow earthquakes, t_r/t_a is larger by about order 10^3 for deep earthquakes, with possible intermediate values for intermediate earthquakes. Assuming $-\Delta\tau_e/\sigma$ does not exceed order of unity, these results indicate that fault constitutive parameter A decreases to very small values for deep earthquakes.

Spatial dependence of earthquake clustering appears to derive from the spatial dependence of the stress changes around a prior earthquake source. Results have been presented for an approximate representation of shear stress change in the plane of a shear crack in an elastic medium. Hence the model specifically applies to alteration of earthquake rates along the plane of the prior earthquake and outside of its rupture area. However, it is reasoned that all stress changes resulting from an earthquake will generally have similar spatial dependence because falloff of stresses by $1/x^3$ is characteristic of finite sources in a three-dimensional body including the shear stress equation (20). Hence distance effects found for the specific model will be generally applicable for perturbation of earthquakes from any stress change resulting from a prior earthquake.

Thus far, only aftershocks lying outside of the zone of the mainshock rupture have been discussed. Many aftershocks originate within the mainshock source region, either on or near to the mainshock rupture surface. Two explanations for these aftershocks appear plausible. First, the aftershocks may occur on patches within the mainshock source region that did not slip during the mainshock. Such patches would experience large stress increases at the time of the mainshock and would therefore have a high potential for aftershocks. The second and favored explanation is that aftershocks within the region of a mainshock may represent adjustments on secondary faults to stresses induced by mainshock slip. In particular, no fault is perfectly planar and consequently mainshock slip will give rise to large local changes of shear and normal stress as nonmatching geometry on opposite sides of the fault interfere [Saucier *et al.*, 1992]. Those stresses will increase with each successive earthquake unless there is bulk flow or slip on secondary faults to relax the stress. Aftershock mechanisms that differ from that of the mainshock and originate near to but not on the mainshock plane [Beroza and Zoback, 1993] may be evidence of this process.

Aftershock decay is generally well represented by $(1/t)^p$ with p ordinarily in the range 0.5–1.5. For the formulation developed here, equations (12) and (13) give $p = 1.0$ if stress change and other model parameters are uniform

over the volume considered. Deviations from $p = 1$ and variability between aftershock sequences will arise from several causes. These include spatial variability of various model parameters over the volume considered and stressing histories not satisfying the simple conditions of (12) and (13). Spatial variability of model parameters requires an appropriately weighted average of the family of curves plotted in Figure 2 and tends to decrease p relative to the homogeneous case. With the exception of stress change it is expected that model parameters ($A, \sigma, r, \dot{\tau}_r$, and $\dot{\tau}$) would probably not vary systematically with respect to distance from the mainshock. Consequently, such effects might tend to cancel and any noncanceling effects would require analysis specific to a particular mainshock (i.e., the effects would not be systematic to all aftershock sequences).

Use of nonuniform stress changes, characteristic of the elastic stresses around a shear crack, yield $p \approx 0.8$ (Figure 5). Comparable decay rates are found for earthquake pair data compiled by *Kagan and Jackson* [1991] and for foreshock-mainshock pairs of *Jones* [1985] which suggest that rates of decay shown in those composite data sets show the systematic effect of the nonuniform elastic stress field near a shear crack.

Another source of variability of p relates to nonconstant stress or stressing rate following an earthquake stress step. Simulations with multiple stress steps, in which the later stress steps represent large aftershocks with secondary aftershock sequences (Figure 7) yield an apparent $p > 1$ during secondary aftershock sequences. Recall that this effect is entirely an artifact of plotting the entire sequence by the logarithm of the time since the mainshock. As shown by Figure 8 relaxation of stresses with time can result in various rates of decay including cases where $p > 1$.

The formulation developed here assumes that seismicity rate in the absence of stress perturbations is independent of time. This steady state assumption appears to be adequate for the applications explored here, at least over time intervals comparable to t_a which is small compared to the mean earthquake recurrence time. Hence for those time intervals the reference seismicity rate is consistent with a Poisson model of earthquake occurrence, and the perturbed seismicity is analogous to that of a nonstationary Poisson model. The introduction of the stochastic element in the formulation relates to the distribution of initial conditions over the population of sources or, equivalently, to the uncertainty in initial conditions on a single source that nucleates a specific earthquake. It is emphasized that the nucleation process is not intrinsically uncertain. The underlying model is of fully deterministic nucleation of earthquake sources in which the stress on each source begins at some low value and increases with time until the conditions for onset of an earthquake are satisfied. Hence conditions on an individual source are consistent with the stressing cycle often assumed for quasiperiodic earthquake occurrence.

In conclusion, it is noted that applications of the seismicity rate constitutive formulation are not restricted to the simple stress step models investigated here. It may be applied to stressing histories of arbitrary complexity such as Earth tides and passage of seismic waves. The demonstrated capability for modeling the space and time characteristics of clustering phenomena suggests the feasibility of using observations of temporal variations of earthquake rate to

invert for changes in driving stress. Also, the formulation presented here could be employed to estimate short- to intermediate-term earthquake probabilities following prior earthquakes. Such probability estimates may serve as an alternative or adjunct to estimates that employ empirically derived relations for earthquake potential analogous to that obtained for this model [e.g., *Jones*, 1985; *Reasenberg and Jones*, 1989; *Working Group*, 1992].

Appendix A: Earthquake Nucleation

Nucleation model. The following summarizes results obtained for a simplified model of a nucleation source that is represented as single spring-slider system. Details of the model and comparison of the simple model with plane strain numerical solutions of a fault with spatially variable conditions are given by *Dieterich* [1992]. Here the spring and slider results of *Dieterich* [1992] are generalized somewhat by incorporation of the multiple state representation of fault friction (equation (5)). Additionally, results are obtained for the change of conditions on a source arising from a step in both shear and normal stress.

Spring stiffness per unit area, k , may be scaled to crack length by

$$k = \frac{\Delta\tau}{\delta} - \frac{G\eta}{l}, \quad (\text{A1})$$

where l is half-length or radius of the fault segment, G is shear modulus (Poisson's ratio of 0.25), and η is a crack geometry parameter with values near 1 [*Dieterich*, 1986, 1992]. For an instability to develop, k must be less than the critical stiffness for unstable slip [*Dieterich*, 1981; *Ruina*, 1983; *Rice and Ruina*, 1983; *Dieterich and Linker*, 1992]. Hence from (A1), critical spring stiffness can be related to a minimum dimension for unstable slip giving

$$l_c = \frac{G\eta D_c}{\xi\sigma}, \quad (\text{A2})$$

where ξ is a parameter that depends on constitutive properties and loading conditions. It is found that the nucleation process is characterized by an interval of self-driven accelerating slip that precedes instability. The duration of the nucleation process is highly sensitive to initial stress and initial θ . The numerical simulations demonstrate that the segment on which instability nucleates also has a characteristic length l_c that scales by (A2). Empirical evaluation of the size of the nucleation zone from the numerical models gives $\xi \sim 0.4B$. If accelerating slip initiates on a patch that exceeds l_c , the zone of most rapid acceleration tends to shrink to the characteristic length as the time of instability approaches.

Equating constitutive law (5) for fault strength with fault stress gives

$$\frac{\tau(t) - k\delta}{\sigma} = \mu_0' + A \ln \dot{\delta} + \sum_{i=1}^n B \ln \theta_i, \quad (\text{A3})$$

where $\tau(t)$ is the remotely applied stress acting on the fault in the absence of slip and $-k\delta$ is the decrease in stress due to fault slip. In (A3) the constant terms μ_0 , $A \ln \delta^*$, and $B_i \ln \theta_i^*$ have been grouped into μ_0' . Normal stress is assumed to be constant. Recall that θ evolves with sliding history as given by equation (6). The problem may be

solved numerically. However, when the nucleation process is underway and slip is accelerating, the slip speed soon greatly exceeds the steady state speed for all θ_i (i.e., $\dot{\theta}_i > D_{ci}/\delta$). As this happens, the $1/\delta$ term in (6) will no longer contribute to the evolution, and (6) can be well approximated by

$$\left(\frac{\partial \theta_i}{\partial \delta} \right)_{\sigma=\text{const}} = -\frac{\theta_i}{D_{ci}}, \quad \theta_i = \theta_{0i} e^{-\delta/D_{ci}}. \quad (\text{A4})$$

Hence state is simply dependent on displacement, where θ_{0i} is state at $\delta = 0$.

For slip at constant normal stress, substitution of (A4) into (A3) yields

$$\frac{\tau(t) - k\delta}{\sigma} = \mu_0' + A \ln \dot{\delta} + \sum_{i=1}^n B_i \ln \theta_{0i} - \delta \sum_{i=1}^n \frac{B_i}{D_{ci}}. \quad (\text{A5})$$

For a variety of functions for the remote stressing term, (A5) yields a separable differential equation that may be solved directly.

Constant stressing rate. For the case of constant rate of remote loading, $\tau(t) = \tau_0 + \dot{\tau}t$, (A5) may be rearranged by solving for $\dot{\delta} = d\delta/dt$ giving

$$\dot{\delta}_0 \int_0^t \exp \left\{ \frac{\dot{\tau}t}{A\sigma} \right\} dt = \int_0^\delta \exp \left\{ \frac{-H\delta}{A} \right\} d\delta, \quad (\text{A6})$$

where $\dot{\delta}_0$ and H contain terms for the initial conditions and model constants, respectively

$$\dot{\delta}_0 = \left[\left(\theta_{01} \right)^{-B_1/A} \left(\theta_{02} \right)^{-B_2/A} \dots \right] \exp \left\{ \frac{\tau_0/\sigma - \mu_0'}{A} \right\} \quad (\text{A7})$$

$$H = -\frac{k}{\sigma} + \sum_{i=1}^n \frac{B_i}{D_{ci}}. \quad (\text{A8})$$

Note in (A7) that the initial slip speed $\dot{\delta}$ fully describes the initial conditions τ_0 and θ_{0i} . Equation (A6) has the following solutions:

$$\delta = \frac{-A}{H} \ln \left\{ \frac{\dot{\delta}_0 H \sigma}{\dot{\tau}} \left[1 - \exp \left(\frac{\dot{\tau}t}{A\sigma} \right) \right] + 1 \right\}, \quad \dot{\tau} \neq 0, \quad (\text{A9})$$

$$\delta = \frac{-A}{H} \ln \left\{ 1 - \frac{\dot{\delta}_0 H t}{A} \right\}, \quad \dot{\tau} = 0. \quad (\text{A10})$$

The slip speeds are

$$\dot{\delta} = \left\{ \left[\frac{1}{\dot{\delta}_0} + \frac{H\sigma}{\dot{\tau}} \right] \left[\exp \left(\frac{-\dot{\tau}t}{A\sigma} \right) \right] - \frac{H\sigma}{\dot{\tau}} \right\}^{-1}, \quad \dot{\tau} \neq 0 \quad (\text{A11})$$

$$\dot{\delta} = \left[\frac{1}{\dot{\delta}_0} - \frac{Ht}{A} \right]^{-1}, \quad \dot{\tau} = 0 \quad (\text{A12})$$

The time of instability, t , is obtained by substituting $\dot{\delta}_i$, the slip speed at instability, into (A11) and (A12). The following employs $1/\dot{\delta}_i = 0$. Use of finite $\dot{\delta}_i$ while tractable,

introduces additional terms into the equations and does not result in solutions that are numerically distinguishable from the simpler solutions provided $\dot{\delta}_i$ is much greater than the average long term fault slip rate. This condition is well satisfied for earthquake processes where $\dot{\delta}_i$ varies from centimeters to meters per second and long-term slip rates are in millimeters to centimeters per year. Time of instability is

$$t = \frac{A\sigma}{\dot{\tau}} \ln \left(\frac{\dot{\tau}}{H\sigma\dot{\delta}_0} + 1 \right), \quad \dot{\tau} \neq 0, \quad (\text{A13})$$

$$t = \frac{A}{H} \left(\frac{1}{\dot{\delta}_0} \right), \quad \dot{\tau} = 0. \quad (\text{A14})$$

The evolution of state on a nucleation source after some time interval is readily obtained from the displacement solution and (A2). The results of (A13) and (A14) are in surprisingly good agreement with the times to instability obtained from detailed numerical simulations of a fault with spatial variation of conditions [Dieterich, 1992].

The above solutions have the useful characteristic that they may be applied repeatedly, in a step-by-step manner, to approximate complicated stressing histories as a series of constant stressing rate increments. Recall that initial slip speed fully describes the initial conditions. Hence the initial slip speed $\dot{\delta}_0$, at the start of each time interval in a loading history, is obtained from the solution for slip speed ((A13) and (A12)) at the end of the previous time interval.

The effects of jumps of normal stress and shear stress on slip speed may be found from the constitutive relations ((A5) and (A6)). Before a stress jump, slip speed depends on initial stress and state as given by (A7). Similarly, the slip speed following the stress jump depends on τ , σ , and θ after the step. Jumps of τ do not affect state, but from (6) change of normal stress from σ_0 to σ results in the change of state

$$\theta_i = \theta_{0i} \left(\frac{\sigma}{\sigma_0} \right)^{-\alpha_i/B_i}. \quad (\text{A15})$$

Hence, from (A7) and (A15), after the stress jump

$$\dot{\delta} = \left[\left(\theta_{01} \right)^{-B_1/A} \left(\theta_{02} \right)^{-B_2/A} \dots \right] \times \left[\left(\frac{\sigma}{\sigma_0} \right)^{\alpha_1/A} \left(\frac{\sigma}{\sigma_0} \right)^{\alpha_2/A} \dots \right] \exp \left\{ \frac{\tau}{A\sigma} - \frac{\mu_0'}{A} \right\}. \quad (\text{A16})$$

By using (A7) the state terms in (A16) may be defined in terms of initial stresses and $\dot{\delta}_0$ giving

$$\dot{\delta} = \dot{\delta}_0 \left(\frac{\sigma}{\sigma_0} \right)^{\alpha/A} \exp \left(\frac{\tau}{A\sigma} - \frac{\tau_0}{A\sigma_0} \right), \quad \alpha = \sum_{i=1}^n \alpha_i. \quad (\text{A17})$$

Appendix B: Formulation for Effect of Stressing History on Earthquake Rate

Distribution of conditions for steady state seismicity. Taking $dn/dt = r$ as the reference rate of seismicity, the time of an earthquake at source n is

$$t = \frac{n}{r}. \quad (\text{B1})$$

In Appendix A, initial slip speed is shown to fully describe the initial conditions for subsequent acceleration of slip to instability (equation (A7)). The distribution of initial conditions over the steady state population of patches is obtained by equating the result for time of instability (A13) with (B1) and rearranging to give initial slip speed as the dependent variable:

$$\dot{\delta}(n) = \frac{1}{\left[\frac{H\sigma}{\dot{\tau}_r} \right] \left[\exp\left(\frac{\dot{\tau}_r n}{A\sigma r}\right) - 1 \right]} , \quad \dot{\tau}_r \neq 0 \quad (\text{B2})$$

where $\dot{\tau}_r$ is the reference stressing rate. Hence the time of instability at the n th source may be found by evaluating (B2) at n to obtain $\dot{\delta}_0$ and then substituting that value into the appropriate solution for time to instability, e.g., equation (A14). For later convenience, (B2) is rewritten as

$$\dot{\delta}(n) = \frac{1}{H\sigma\gamma \left[\exp\left(\frac{\dot{\tau}_r n}{A\sigma r}\right) - 1 \right]} \quad (\text{B3})$$

Hence for the reference steady state distribution, $\gamma = 1/\dot{\tau}_r$. Below, the effects of stressing history on the distribution (B3) are examined. It is shown that the distribution of slip speeds is always of the form of (B3) but with different values of γ that evolve with stressing history.

Evolution equation for distribution. The general equation for evolution of γ is found by evaluating the partial derivatives in

$$d\gamma = \left(\frac{\partial \gamma}{\partial t} \right)_{\tau,\sigma} dt + \left(\frac{\partial \gamma}{\partial \tau} \right)_{t,\sigma} d\tau + \left(\frac{\partial \gamma}{\partial \sigma} \right)_{t,\tau} d\sigma . \quad (\text{B4})$$

To find $(\partial \gamma / \partial t)_{\tau,\sigma}$ the distribution $\dot{\delta}(n)$ of equation (B3) is substituted for $\dot{\delta}_0$ in (A12) giving the distribution of slip speeds after some elapsed time t at $\dot{\tau} = 0, \dot{\sigma} = 0$,

$$\dot{\delta}(n) = \frac{1}{H\sigma\gamma_0 \left[\exp\left(\frac{\dot{\tau}_r n}{A\sigma r}\right) - 1 \right] - \frac{Ht}{A}} . \quad (\text{B5})$$

The use of γ_0 indicates the value of γ at $t = 0$. After time t has elapsed, some number of sources, I , will have nucleated earthquakes because the speed for onset of instability $\dot{\delta}_i$ has been reached. Consequently, those sources will no longer be a part of the population. Setting $\dot{\delta}(n) = \infty$ and $n = I$ in (B5) and solving for I gives

$$I = \frac{A\sigma r}{\dot{\tau}_r} \ln \left[1 + \frac{t}{\gamma A\sigma} \right] . \quad (\text{B6})$$

The updated distribution of slip speeds, after time increment t , is obtained by the substitution $I + n = n_{\text{old}}$ in (B5), where n_{old} now refers to n appearing in (B5), prior to the time step and using (B6) to evaluate I . Following some algebra, the new evolved distribution is found to have the form of (B3) as previously asserted with

$$\gamma = \gamma_0 + \frac{t}{A\sigma} , \quad (\text{B7})$$

which gives

$$\left(\frac{\partial \gamma}{\partial t} \right)_{\tau,\sigma} = \frac{1}{A\sigma} . \quad (\text{B8})$$

A similar procedure is used to evaluate $(\partial \gamma / \partial \tau)_{t,\sigma}$ and $(\partial \gamma / \partial \sigma)_{t,\tau}$. From (B3) and (A17) the distribution of slip speeds following a step in shear stress and normal stress is

$$\dot{\delta}(n) = \frac{\left(\frac{\sigma}{\sigma_0} \right)^{\alpha/A} \exp\left(\frac{\tau}{A\sigma} - \frac{\tau_0}{A\sigma_0}\right)}{H\sigma\gamma \left[\exp\left(\frac{\dot{\tau}_r n}{A\sigma r}\right) - 1 \right]} . \quad (\text{B9})$$

Figure 1 illustrates the effect of a stress step on the distribution. A stress step that increases slip speed (an increase of shear stress or decrease of normal stress) will cause some number of patches, I , to nucleate earthquakes if the slip speed $\dot{\delta}_i$ at instability is finite. Setting $\dot{\delta} = \dot{\delta}_i$ in (B9) and solving for the number sources, I , that have nucleated an earthquake gives

$$I = \frac{A\sigma r}{\dot{\tau}_r} \ln \left\{ 1 + \frac{1}{\gamma_0} \left[(H\sigma\dot{\delta}_i)^{-1} \left(\frac{\sigma}{\sigma_0} \right)^{\alpha/A} \right] \exp\left(\frac{\tau}{A\sigma} - \frac{\tau_0}{A\sigma_0}\right) \right\} . \quad (\text{B10})$$

The new distribution of conditions following the stress step is obtained by the substitution, $I + n = n_{\text{old}}$, in (B9) and using (B10) to evaluate I . Use of either finite or infinite $\dot{\delta}_i$ at instability again yields an evolved distribution of the form of (B3) with

$$\gamma = \gamma_0 \left(\frac{\sigma}{\sigma_0} \right)^{-\alpha/A} \exp\left(\frac{\tau_0}{A\sigma_0} - \frac{\tau}{A\sigma}\right) , \quad (\text{B11})$$

where γ_0 denotes the value of γ immediately prior to the stress step. From this result

$$\left(\frac{\partial \gamma}{\partial \tau} \right)_{t,\sigma} = \frac{-\gamma}{A\sigma} , \quad (\text{B12})$$

and

$$\left(\frac{\partial \gamma}{\partial \sigma} \right)_{t,\tau} = \frac{\gamma\tau}{A\sigma^2} - \frac{\gamma\alpha}{A\sigma} . \quad (\text{B13})$$

In summary, the distribution of slip speeds retains the form of (B3) through time (with $\dot{\tau} = 0, \dot{\sigma} = 0$) and through steps in shear and normal stress. Because any loading history may be represented as a sequence of sufficiently small stress jumps and time steps (with $\dot{\tau} = 0, \dot{\sigma} = 0$), the distribution of slip speeds will retain the form of (B3) for any stressing history. From (B4), (B8), (B12), and (B13) the general evolution equation for γ is

$$d\gamma = \frac{1}{A\sigma} \left[dt - \gamma d\tau + \gamma \left(\frac{\tau}{\sigma} - \alpha \right) d\sigma \right] . \quad (\text{B14})$$

Recall from (A17) that $\alpha = \alpha_1 + \alpha_2 + \dots$ for applications employing friction formulations with multiple state variables.

Solutions for linear and logarithmic shear stress-ing. Solution of (B14) for change of γ for increase of shear stress at a constant rate and by logarithm of time are easy

to obtain and of use for modeling earthquake processes. If shear stress is given by

$$\tau = \tau_0 + \dot{\tau}t, \quad (B15)$$

and $\dot{\sigma} = 0$, then from (B14), evolution of γ is given by

$$d\gamma = \frac{1}{A\sigma}[1 - \gamma\dot{\tau}]dt, \quad (B16)$$

which has the solution

$$\gamma = \left[\gamma_0 - \frac{1}{\dot{\tau}} \right] \exp \left[\frac{-t\dot{\tau}}{A\sigma} \right] + \frac{1}{\dot{\tau}}. \quad (B17)$$

For logarithmic stressing,

$$\tau = \tau_0 + u \ln(wt + 1), \quad (B18)$$

and $\dot{\sigma} = 0$, the evolution equation (B14) becomes

$$d\gamma = \frac{1}{A\sigma} \left[1 - \frac{\gamma uw}{bt + 1} \right] dt. \quad (B19)$$

Using the integrating factor

$$(wt + 1)^m, \text{ where } m = \frac{u}{A\sigma}, \quad (B20)$$

(B19) has the solution

$$\gamma = \gamma_0(wt + 1)^{-m} + \frac{(wt + 1) - (wt + 1)^{-m}}{A\sigma w(m + 1)}. \quad (B21)$$

These solutions may also be obtained using the procedure of the previous section which evolves the distribution of initial slip speeds by employing the specific solutions for increase of slip speed with time of a source. Conversely, the earlier solutions for evolution of γ for constant stress and for stress steps, equations (B7) and (B11), respectively, may of course be obtained by direct solution of (B14).

Seismicity rate. Under the condition $\dot{\tau} = 0, \dot{\sigma} = 0$, the distribution of earthquakes times beginning at $t = 0$ is found from (A14) by substituting the distribution of slip speeds (B3) for initial slip speed δ_0 . In making this substitution, note that the distribution of initial speeds is fixed at $t = 0$ and, consequently, γ is fixed at γ_0 . The distribution of times of earthquakes is

$$t = A\sigma\gamma_0 \left[\exp \left(\frac{\dot{\tau}_r n}{A\sigma r} \right) - 1 \right], \dot{\tau} = 0, \dot{\sigma} = 0. \quad (B22)$$

Rearranging for n ,

$$n = \frac{A\sigma r}{\dot{\tau}_r} \ln \left[\frac{t}{A\sigma\gamma_0} + 1 \right], \dot{\tau} = 0, \dot{\sigma} = 0, \quad (B23)$$

and differentiating gives seismicity rate $R = dn/dt$ normalized by the reference rate r

$$\frac{R}{r} = \frac{1/\dot{\tau}_r}{\gamma_0 + \frac{t}{A\sigma}}, \dot{\tau} = 0, \dot{\sigma} = 0. \quad (B24)$$

Note that the denominator of the solution for seismicity rate is simply the specific solution of $\gamma(t)$ given in (B7) for these

stressing conditions ($\dot{\tau} = 0, \dot{\sigma} = 0$).

This suggests

$$R = \frac{r}{\gamma\dot{\tau}_r} \quad (B25)$$

as a general formulation for any stressing history. Hence, it is proposed that at any instant seismicity rate depends on the current value of γ and is independent of current stressing rate. The validity of (B25) for any stressing history may be understood by considering the nucleation process during unconstrained loading histories. As implied by (B4) and as discussed previously, the evolution of γ for any loading history may be found by breaking the loading history into a series of sufficiently small stress jumps and time increments with $\dot{\tau} = 0, \dot{\sigma} = 0$. Because γ determines the initial conditions for the time to instability, (B25) will be generally valid if the time to instability becomes independent of stressing rate as time decreases to zero. The solutions for time of instability for $\dot{\tau} = 0$ (equation (A13)) and for $\dot{\tau} \neq 0$ (equation (A14)) converge and become independent of stressing rate as slip speed approaches the critical speed for instability demonstrating that this condition is satisfied. Indeed, (B25) may be obtained by the following the above procedures with solutions for time to instability and evolution of γ under conditions where stressing rate is not zero (i.e., $\tau = \tau_0 + \dot{\tau}t, \dot{\sigma} = 0$ and $\tau = \tau_0 + u \ln(wt + 1), \dot{\sigma} = 0$).

Equations (B14) and (B25) compose the general formulation for stressing history dependence of seismicity rates.

Acknowledgments: This study profited from discussions with numerous people over a period of several years. I especially wish to acknowledge the assistance provided by Mike Blanpied, John Dvorak, John Lahr, Paul Okubo, Paul Reasenberg, Bob Simpson, and Will Tanigawa. Joe Andrews, Mark Linker, Jim Savage, George Sutton, John Weeks, and Max Wyss provided reviews and several useful suggestions.

References

- Beroza, G. C., and M. D. Zoback, Mechanism diversity in the Loma Prieta aftershocks and mechanics of mainshock-aftershock interactions, *Science*, 259, 210–213, 1993.
- Blanpied, M. L., and T. E. Tullis, The stability and behavior of a frictional system with a two state variable constitutive law, *Pure Appl. Geophys.*, 124, 415–444, 1986.
- Blanpied, M. L., D. A. Lockner, and J. D. Byerlee, Fault stability inferred from granite sliding experiments at hydrothermal conditions, *Geophys. Res. Lett.*, 18, 609–612, 1991.
- Dieterich, J. H., Modeling of rock friction, 1, Experimental results and constitutive equations, *J. Geophys. Res.*, 84, 2161–2168, 1979a.
- Dieterich, J. H., Modeling of rock friction, 2, Simulation of preseismic slip, *J. Geophys. Res.*, 84, 2169–2175, 1979b.
- Dieterich, J. H., Constitutive properties of faults with simulated gouge, in *Mechanical Behavior of Crustal Rocks*, *Geophys. Monogr. Ser.*, vol. 24, edited by N. L. Carter, M. Friedman, J. M. Logan, and D. W. Stearns, pp. 103–120, AGU, Washington, D. C., 1981.
- Dieterich, J. H., A model for the nucleation of earthquake slip, in *Earthquake Source Mechanics*, *Geophys. Monogr. Ser.*, vol. 37, edited by S. Das, J. Boatwright, and C. H. Scholz, pp. 37–47, AGU, Washington, D. C., 1986.

- Dieterich, J. H., Nucleation and triggering of earthquake slip: Effect of periodic stresses, *Tectonophysics*, 144, 127–139, 1987.
- Dieterich, J. H., Growth and persistence of Hawaiian volcanic rift zones, *J. Geophys. Res.*, 93, 4258–4270, 1988a.
- Dieterich, J. H., Probability of earthquake recurrence with non-uniform stress rates and time-dependent failure, *Pure Appl. Geophys.*, 126, 589–617, 1988b.
- Dieterich, J. H., Earthquake nucleation on faults with rate and state-dependent friction, *Tectonophysics*, 211, 115–134, 1992.
- Dieterich, J. H., and M. F. Linker, Fault stability under conditions of variable normal stress, *Geophys. Res. Lett.*, 19, 1691–1694, 1992.
- Dvorak, J. J., A. T. Okamura, T. T. English, R. Y. Koyanagi, J. S. Nakata, M. R. Sako, W. T. Tanigawa, and K. M. Yamashita, Mechanical response of the south flank of Kilauea volcano, Hawaii, to intrusive events along the rift systems, *Tectonophysics*, 124, 193–209, 1986.
- Ellsworth, W. L., and L. D. Dietz, Repeating earthquakes: Characteristics and implications, in Proceedings of Workshop XLVI, The 7th U. S.-Japan Seminar on Earthquake Prediction, *U.S. Geol. Surv. Open File Rep.*, 90-98, 226–245, 1990.
- Ellsworth, W. L., A. G. Lindh, W. H. Prescott, and D. G. Herd, The 1906 San Francisco earthquake and the seismic cycle, in *Earthquake Prediction: An International Review, Maurice Ewing Volume 4*, edited by D. W. Simpson and P. G. Richards, pp. 126–140, AGU, Washington, D. C., 1981.
- Frolich, C., Aftershocks and temporal clustering of deep earthquakes, *J. Geophys. Res.*, 92, 13,944–13,956, 1987.
- Jones, L. M., Foreshocks (1966–1980) in the San Andreas system, California, *Bull. Seismol. Soc. Am.*, 74, 1361–1380, 1984.
- Jones, L. M., Foreshocks and time-dependent earthquake hazard assessment in southern California, *Bull. Seismol. Soc. Am.*, 75, 1669–1679, 1985.
- Jones, L. M., and P. Molnar, Some characteristics of foreshocks and their possible relation to earthquake prediction and premonitory slip, *J. Geophys. Res.*, 84, 5709–5723, 1979.
- Kagan, Y. Y., and D. D. Jackson, Long-term earthquake clustering, *Geophys. J. Int.*, 104, 117–133, 1991.
- Kirby, S. H., W. B. Durham, and L. A. Stern, Mantle phase changes and deep-earthquake faulting in subducting lithosphere, *Science*, 252, 216–225, 1991.
- Linker, M. F., and J. H. Dieterich, Effects of variable normal stress on rock friction: Observations and constitutive equations, *J. Geophys. Res.*, 97, 4923–4940, 1992.
- Marone, C. J., C. H. Scholz, and R. Bilham, On the mechanics of earthquake afterslip, *J. Geophys. Res.*, 96, 8441–8452, 1991.
- Matsu'ura, M., D. D. Jackson, and A. Cheng, Dislocation model for aseismic crustal deformation at Hollister, California, *J. Geophys. Res.*, 91, 12,661–12,674, 1986.
- Ogata, Y., and K. Shimazaki, Transition from aftershocks to normal activity: The 1965 Rat Islands earthquake aftershock sequence, *Bull. Seismol. Soc. Am.*, 74, 1757–1765, 1984.
- Okubo, P. G., Dynamic rupture modeling with laboratory derived constitutive relations, *J. Geophys. Res.*, 94, 12,321–12,336, 1989.
- Okubo, P. G., and J. H. Dieterich, State variable fault constitutive relations for dynamic slip, in *Earthquake Source Mechanics, Geophys. Monogr. Ser.*, vol. 37, edited by S. Das, J. Boatwright, and C. H. Scholz, pp. 25–35, AGU, Washington, D. C., 1986.
- Reasenberg, P., and W. L. Ellsworth, Aftershocks of the Coyote Lake, California, earthquake of August 6, 1979: A detailed study, *J. Geophys. Res.*, 87, 10,637–10,655, 1982.
- Reasenberg, P. A., and L. M. Jones, Earthquake hazard after a mainshock in California, *Science*, 243, 1173–1176, 1989.
- Reasenberg, P. A., and R. W. Simpson, Response of regional seismicity to the static stress change produced by the Loma Prieta earthquake, *Science*, 255, 1687–1690, 1992.
- Rice, J. R., and J.-C. Gu, Earthquake aftershocks and triggered seismic phenomena, *Pure Appl. Geophys.*, 121, 187–219, 1983.
- Rice, J. R., and A. L. Ruina, Stability of steady frictional slipping, *J. Appl. Mech.*, 50, 343–349, 1983.
- Ruina, A. L., Slip instability and state variable friction laws, *J. Geophys. Res.*, 88, 10,359–10,370, 1983.
- Saucier, F., E. Humphreys, and R. Weldon, Stress near geometrically complex strike-slip faults: Application to the San Andreas fault at Cajon Pass, southern California, *J. Geophys. Res.*, 97, 5081–5094, 1992.
- Scholz, C. H., The critical slip distance for seismic faulting, *Nature*, 336, 761–763, 1988.
- Stein, R. S., and M. Lisowski, The 1979 Homestead Valley earthquake sequence, California: Control of aftershocks and postseismic deformation, *J. Geophys. Res.*, 88, 6477–6490, 1983.
- Stuart, W. D., Forecast model for great earthquakes at the Nankai trough subduction zone, *Pure Appl. Geophys.*, 126, 619–641, 1988.
- Tajima, F., and H. Kanamori, Global survey of aftershock area expansion patterns, *Phys. Earth Planet. Inter.*, 40, 77–134, 1985.
- Tse, S. T., and J. R. Rice, Crustal earthquake instability in relationship to the depth variation of frictional slip properties, *J. Geophys. Res.*, 91, 9452–9472, 1986.
- Tsukuda, T., Long-term seismic activity and present microseismicity on active faults in southwest Japan, paper presented at U.S.-Japan Seminar on Practical Approaches to Earthquake Prediction and Warning, Tokyo and Tsakuba, Japan, November 7–11, 1983.
- Tullis, T. E., and J. D. Weeks, Constitutive behavior and stability of frictional sliding of granite, *Pure Appl. Geophys.*, 124, 383–314, 1986.
- Utsu, T., Aftershocks and earthquake statistics (I), *J. Fac. Sci., Hokkaido Univ., Ser. 7*, 3, 129–195, 1969.
- Weeks, J. D., and T. E. Tullis, Frictional sliding of dolomite: A variation in constitutive behavior, *J. Geophys. Res.*, 90, 7821–7826, 1985.
- Wesson, R. L., Modelling aftershock migration and afterslip of the San Juan Bautista, California, earthquake of October 3, 1972, *Tectonophysics*, 144, 214–229, 1987.
- Working Group, Probabilities of large earthquakes in the San Francisco Bay region, California, *U.S. Geol. Surv. Circ.*, 1053, 51 pp., 1990.
- Working Group, Future seismic hazards in southern California, Phase I: Implications of the 1992 Landers earthquake sequence, report, Cal. Div. of Mines and Geol., Sacramento, 1992.
- Wyss, M., Regular recurrence intervals between Hawaiian earthquakes: Implications for predicting the next event, *Science*, 234, 726–728, 1986.
- Wyss, M., A proposed model for the great Kau, Hawaii, earthquake of 1868, *Bull. Seismol. Soc. Am.*, 78, 1450–1462, 1988.
- Wyss, M., and R. E. Haberman, Precursory seismic quiescence, *Pure Appl. Geophys.*, 126, 319–332, 1988.

J.H. Dieterich, U.S. Geological Survey, 345 Middlefield Road, MS/977, Menlo Park, CA 94025.

(Received March 11, 1993; revised September 2, 1993; accepted September 8, 1993.)